

HEAT TRANSFER CHARACTERISTICS OF A NON-ROTATING TWO-PASS RECTANGULAR DUCT WITH VARIOUS GUIDE VANES IN THE TIP TURN REGION

Dong Myeong Lee ^a, Jun Su Park ^a, Dong Hyun Lee ^a, Beom Soo Kim ^b and Hyung Hee Cho^{a†}

^aDepartment of Mechanical Engineering Yonsei University, Seoul, 120-749, Korea
E-mail: hhcho@yonsei.ac.kr

^bKorea Electric Power Research Institute. Daejeon, 305-380, Korea

ABSTRACT

The present study investigated convective heat transfer inside a two-pass rectangular duct with guide vanes in the turning region. The objective was to determine the effect of the guide vanes on blade tip cooling. The duct had a hydraulic diameter (D_h) of 26.67 mm and an aspect ratio (AR) of 5. The duct inlet width was 80 mm, and the distance between the tip of the divider and the tip wall of the duct was also 80 mm. Various guide vane configurations were used in the turning region. The Reynolds number (Re), based on the hydraulic diameter, was held constant at 10,000. The naphthalene sublimation technique was used to determine the detailed local heat transfer coefficients, using the heat and mass transfer analogy. The results indicated that guide vanes in the turning region enhanced heat transfer in the blade tip region. The guide vane on the second-pass side of the turning region had higher heat transfer than the guide vane on the first-pass side. Strong secondary flow enhanced heat transfer in the blade tip region. Dean vortices induced by the guide vanes pushed the high-momentum core flow towards the tip wall, and heat transfer was increased in the turning region, but decreased in the second passage. Consequently, a guide vane on the second-pass side of the turning region generates high heat transfer rates on the tip surface, and can also increase the thermal performance factor in a two-pass duct.

Keywords: Turbine internal passage, Blade tip cooling, Turning region, Guide vane, Dean vortex

INTRODUCTION

The inlet temperatures of gas turbine engines have been steadily increasing, for the sake of enhanced thermodynamic efficiency and thrust. Turbine blades are exposed to high-temperature gases, and experience severe thermal stress and

fatigue as a result. Accordingly, increased turbine inlet temperatures have been achieved via better cooling of the turbine blades. Blade cooling should include all regions exposed to high-temperature gas and thermal loads.

In particular, the tips of gas turbine blades experience large thermal loads because of tip leakage flow, resulting in blade tip breakage. The characteristics of blade tip leakage flow in turbines have been investigated extensively, and the basic tip leakage flow mechanism, as well as its effects on aerodynamics and heat transfer in turbomachinery, are effectively summarized and explained by Lakshminarayana [1]. Thermal loads and stresses are concentrated at the tip edges of the rotor blades, and can cause cracks and breakage. It is thus important to cool the tip region. Unfortunately, the tip region is a difficult region to cool. Usually, it is cooled by external film cooling through holes on the blade tips. However, this type of cooling causes turbine power and aerodynamic loss. Additionally, the differences between the internal and external heat transfer rates in the tip region can cause damage. Thus, internal cooling is also necessary to cool the tip region.

Previous studies of internal cooling have attempted to enhance heat transfer on the leading and trailing surfaces. The effects of actual operating conditions, such as rotating conditions, have also been investigated. And, many of studies were reviewed by Bunker [2] and Sunden et al. [3]. Park et al. [4] and Han et al. [5] measured the heat transfer in a stationary duct with a controlled aspect ratio ranging from 0.25 to 4.0, for various rib angles and Reynolds numbers. They concluded that increasing the aspect ratio enhanced the heat transfer in a ribbed duct with a 90° rib angle. Cardone et al. [6] and Astarita et al. [7] measured the characteristics of the turning region and the heat transfer coefficient in a stationary two-pass smooth duct with various aspect ratios, ranging from 1.0 to 5.0, using TLC. Their results showed that the heat transfer rate increased at the outer wall of the second passage after the turning region, due to the high aspect ratio. Mochizuki et al. [8] obtained

detailed measurements of the local heat transfer coefficients in a turbulent flow through smooth and rib-roughened serpentine passages with a sharp 180° bend, and performed flow visualization to reveal the generation of secondary flows. It was found that in a smooth channel, heat transfer downstream from the bend was controlled by secondary flows, and the heat transfer coefficients on the wall surfaces differed from one another. In a ribbed channel, heat transfer in the bend and the second passage can be strongly affected by the ribs, due to the interaction of two secondary flows created by the ribs and the bend. Kim et al. [9-12] measured the local heat/mass transfer and pressure drop in a rotating two-pass duct with transverse ribs. The results showed that the Sherwood number ratios and pressure coefficients were high on the trailing surface in the first passage and the leading surface in the second passage, due to the rotation of the duct. In the turning region of the stationary duct, a pair of Dean vortices were transformed into one large asymmetric vortex cell, changing the heat/mass transfer and pressure drop characteristics. Kim et al. [13] also observed conceptual secondary flow structures in a two-pass duct. Cho et al. [14] measured the detailed heat/mass transfer in a two-pass duct with cross ribs. They concluded that the secondary flow at the end of the turn generated the turning effect in the stationary case. Zehnder et al. [15] measured the pressure loss and heat transfer distribution in a rectangular two-pass channel, to investigate the influence of different turning vane configurations. They concluded that the turning vane configuration had a significant influence on pressure loss and heat transfer in the bend region and the outlet passage. When an appropriate turning vane configuration was used, the pressure loss was reduced by about 25% while the heat transfer remained at nearly the same level in the bend region.

Recently, there have been several studies on cooling the internal tip surfaces of turbine blades. Bunker [16] demonstrated a method that provided substantially increased convective heat flux to the internal tip surfaces. The new tip surface augmentation consisted of several variations involving the fabrication or placement of arrays of discretely shaped pins on the internal tip surface. Five test surfaces were considered, and the results showed that effective heat transfer coefficients based on the original smooth surface area could be increased by up to a factor of 2.5. However, this technique resulted in a negligible increase in the tip turn pressure drop compared with that of a smooth surface. Tareq et al. [17] measured the heat transfer and pressure drop across the outer wall of the bend section (tip side) of a U-duct with smooth and ribbed bends. Xie et al. [18] investigated numerically heat transfer enhancement on a hemispherical dimpled or protruded tip in a rectangular two-pass channel at high Reynolds numbers. In their research, the heat transfer coefficient of the augmented tip was higher, by a factor of 2.0, than that of a smooth tip, due to the combination of turning impingement and protrusion cross flow or dimple advection. This augmentation was achieved at the cost of a pressure drop of around 5%.

Most of the existing studies of internal two-pass cooling have focused on trailing and leading surfaces or the turning

region. However, heat transfer in the internal blade tip region is comparatively unknown and has received little attention. Several studies on internal cooling of the blade tips have recently been conducted. As mentioned above, it is both important and difficult to cool the internal tip region. Thus, the primary objective of this study was to investigate the detailed heat transfer distribution on internal tip surfaces with and without guide vanes in the turning region, using local mass transfer measurements based on the naphthalene sublimation technique. Detailed local heat transfer data are useful for estimating the temperature and thermal stress on a blade tip. These will help to design the blade tip for reducing and preventing crack and failure.

EXPERIMENTAL APPARATUS

Wind Tunnel and Test Channel

Figure 1 shows a schematic of the experimental setup. The apparatus consists essentially of two parts: a flow system that blows air into the test section and a measuring system that records electrical output signals from the duct [19]. Room air flows from a blower to the test duct through a heat exchanger that regulates the air temperature, an orifice flow meter that monitors the flow rate, and a plenum chamber on the top of a rotating seal. The output of the blower is regulated by a frequency controller. To measure the naphthalene surface temperature accurately, J-type thermocouples were embedded in the test plate. The temperature of the bulk air was also measured by thermocouples installed in the channel inlet. An ice bath was used as the thermocouple reference junction. Output signals were recorded using a Hewlett-Packard data logger, interfaced to a computer via slip rings. The test channel consists of the three measuring components shown in Figure 2. Photographs of the measuring components are shown in Figure 3. The two-pass ducts shown in Figure 3 were made of aluminum. The duct width (W) and height (H) were 80 mm and 16 mm, respectively. An aspect ratio (W/H) of 5.0 was maintained with a fixed hydraulic diameter (D_h) of 26.7 mm.

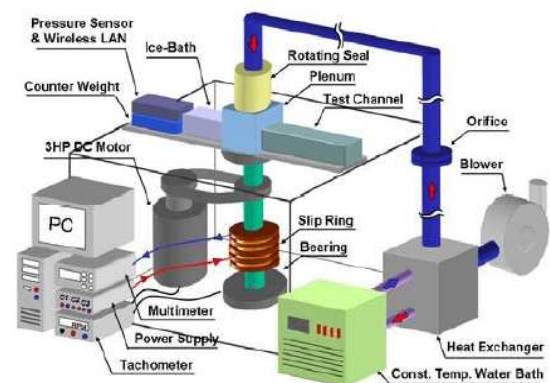


Figure 1. Schematic views of experimental apparatus. [19]

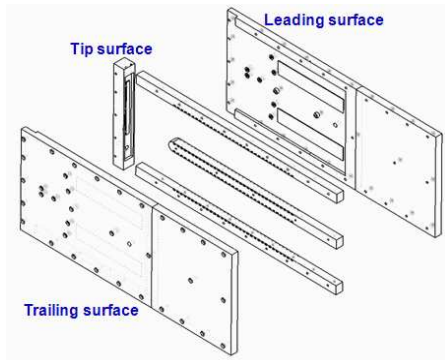


Figure 2. Composition of test channel.

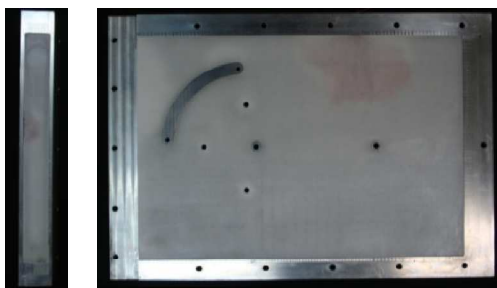


Figure 3. Photographs of test plates.

The inner wall thickness was $0.749D_h$, and the tip had a rounded shape. The distance from the tip to the outer wall was fixed at $1W$. 90° -angled rib turbulators were installed on the leading and trailing surfaces of the first and second passages.

Each rib turbulator had a square cross-section of 1×1 mm. The rib-pitch-to-rib-height ratio (p/e) was 9, and the rib-height-

to-hydraulic-diameter ratio (e/D_h) was 0.0375. The distance from the duct inlet to the starting point of the naphthalene surface was $7D_h$, to attain a fully developed turbulent flow with a secondary flow from the rib turbulators. The radii of the inner and outer guide vanes in the turning region were $1D_h$ and $2D_h$, respectively, measured from the center of the half circle on the tip of the divider wall. Five types of guide vanes and rib turbulators were arranged as shown in Figure 4. The naphthalene sublimation method was used to measure the detailed heat/mass transfer coefficients, using the analogy between heat and mass transfer. The measuring surfaces were coated with naphthalene to simulate the two-sided surface heating conditions of gas turbine blades (the boundary condition of the naphthalene-coated surfaces corresponds to a uniform wall temperature, and that of the inactive surfaces to an adiabatic wall in heat transfer experiments). The temperature of the naphthalene surfaces was accurately measured using the J-type thermocouples installed on the test plates, because the vapor density of naphthalene is temperature-sensitive, and varies approximately 10% per temperature change of 1°C . The coordinate system is shown in Figure 5. The streamwise, lateral and vertical directions correspond to the x -, y -, and z -axes, respectively. The mass transfer measurement domain was covered with naphthalene. The ribbed area of the naphthalene surface extended from $x/D_h = -7.1$ (the starting point of the naphthalene surface in the first passage) to $x/D_h = 7.1$ (the terminal point in the second passage) in the streamwise direction along the outer wall. The domain in the lateral direction (from the outer wall of the first passage to the outer wall of the second passage) extended from $y/D_h = 0$ to $y/D_h = 7.1$. The tip area of the naphthalene surface extended from $y/D_h = 0$ to $y/D_h = 7.1$ in the lateral direction along the tip wall. The domain in the vertical direction (from the leading surface to the

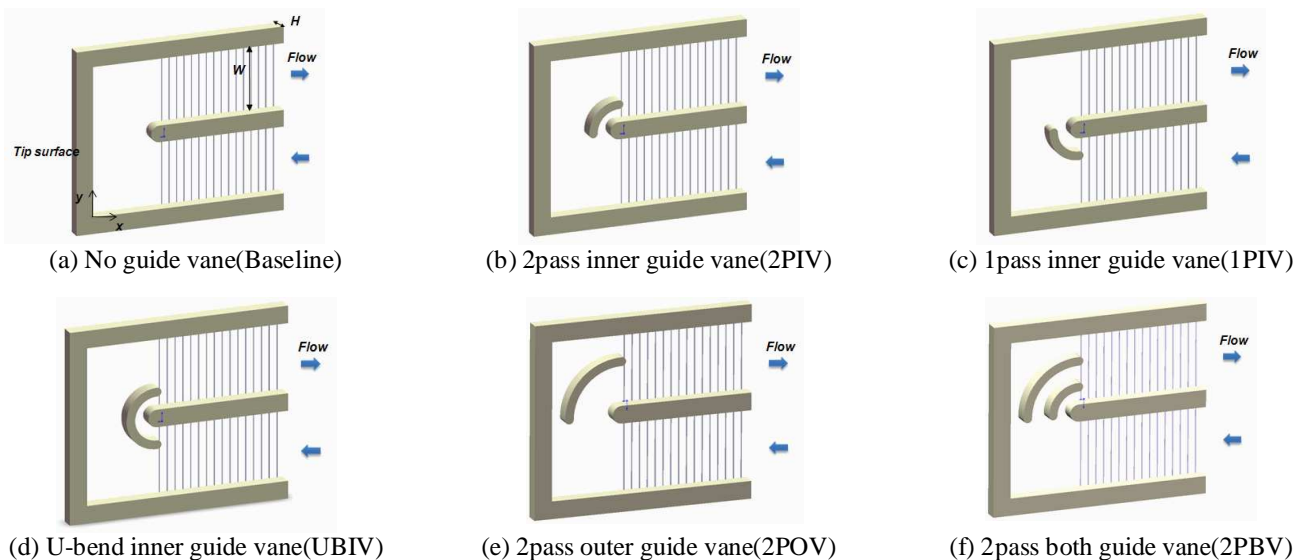


Figure 4. Test channel for various guide vanes.

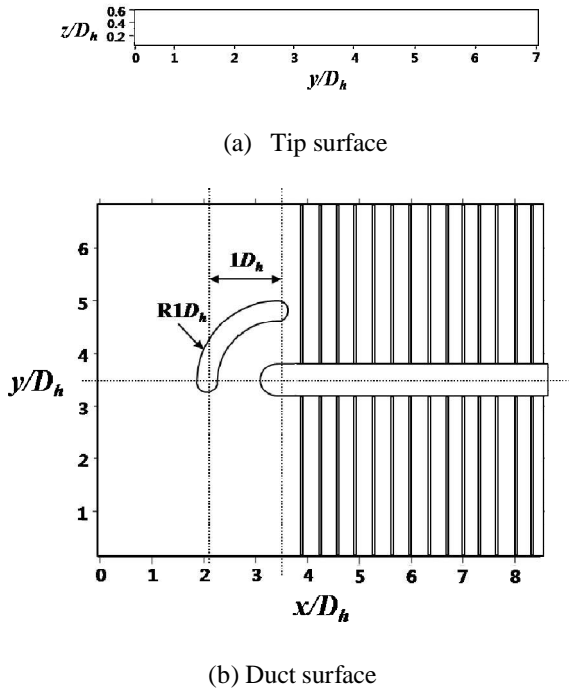


Figure 5. The coordinate system.

trailing surface on the tip wall) extended from $z/D_h = 0$ to $z/D_h = 0.6$. A bell mouth (contraction nozzle) was used to make the inlet velocity profile uniform in the mass transfer experiments. The nominal mean velocity (U) through the test duct was about 5.9 m/s, so that the Reynolds number, based on the hydraulic diameter, is about 10,000. The coolant air was expelled to the atmosphere after the second pass. The pressure drop is measured in the channels using a differential pressure sensor.

PROCEDURE AND DATA REDUCTION

Data Reduction

The naphthalene sublimation method was used to measure the detailed local transfer coefficients on the surface. The three surfaces inside the two-pass duct (i.e., the tip surface and the leading/trailing surfaces) were coated with naphthalene, except for the circumferential edges, which were used as reference points. The local naphthalene sublimation depth was measured to obtain the mass transfer coefficients on the test surfaces, using a linear variable differential transformer (LBB-375TA-020) and an automated positioning table. There were 2,295 measurement points on the tip surface and 10,147 measurement points on the leading and trailing surfaces, including the reference points. The mass transfer coefficient can be expressed as

$$h_m = \frac{\dot{m}}{\rho_{v,w} - \rho_{v,b}} = \frac{\rho_s(\Delta z/\Delta t)}{\rho_{v,w} - \rho_{v,b}} \quad (1)$$

where \dot{m} is the local mass transfer rate of naphthalene per unit area, determined from the density of solid naphthalene (ρ_s) and the sublimation rate ($\Delta z/\Delta t$), and $\rho_{v,w}$ and $\rho_{v,b}$ are the density of the naphthalene vapor on the surface and bulk air, respectively. The former can be calculated from the ideal gas law, using the vapor pressure and the surface temperature:

$$\rho_{v,w} = \frac{P_{naph}}{R_{naph}T_w} \quad (2)$$

The naphthalene vapor pressure P_{naph} was determined from the equation suggested by Ambrose et al. [20]. The bulk vapor density of naphthalene ($\rho_{v,b}$) was obtained from the average naphthalene sublimation depth ($z_{sub}|_x$) measured at each position in the streamwise direction:

$$\rho_{v,b} = \frac{\rho_s W}{\dot{Q}_{air} \Delta t} z_{sub}|_x \quad (3)$$

The Sherwood number was calculated from the local mass transfer coefficient:

$$Sh = h_m D_h / D_{naph} \quad (4)$$

where D_{naph} is the diffusion coefficient of naphthalene in air. This study used properties of naphthalene suggested by Ambrose et al. [20] and Goldstein and Cho [21].

The mass transfer coefficient can be converted to the heat transfer coefficient using the heat and mass transfer equivalence

$$Nu/Sh = (Pr/Sc)^n \quad (5)$$

Most of the mass transfer results are presented in terms of the Sherwood number ratio, Sh/Sh_0 , to assess the heat/mass transfer augmentation. Sh_0 is the Sherwood number for a fully developed turbulent flow in a stationary smooth channel, and its value can be obtained from a well-known correlation of McAdams [22]:

$$Sh_0 = 0.023 Re_{D_h}^{0.8} Sc^{0.4} \quad (6)$$

Sh_0 is the same in all cases, even though the hydraulic diameter varies, because the Reynolds number, based on the hydraulic diameter, was fixed at 10,000. The pitch-averaged Sherwood number, Sh_p , was calculated by integrating the local Sherwood numbers weighted by the pitch-to-pitch area. The span-wise average Sherwood number, Sh_s , was calculated by integrating the local Sherwood numbers in the vertical direction. The uncertainty in the Sherwood number was estimated to be within $\pm 7.76\%$ at a 95% confidence level, using the uncertainty estimation method of Moffat [23].

The friction factors are calculated from measured pressure differences between the inlet and outlet of the test channel.

$$f = \Delta P / [4(\Delta L/D_h)(1/2)\rho U^2] \quad (7)$$

The uncertainty of the friction factor is within 4.4%. The friction loss results are presented as the friction factor ratios, f/f_0 , where f_0 represents the friction factor for a fully developed turbulent flow in a stationary smooth circular tube. The empirical equation that closely fits the Kármán-Nikuradse equation proposed by Petukhov [24] is employed as

$$f_0 = 2(2.236 \ln Re - 4.639)^{-2} \quad (8)$$

The thermal performance, η , which is obtained by considering both the heat/mass transfer augmentation and the friction loss increment is presented based on the constant pumping power condition and it is expressed as the follows [25]:

$$\eta = (\overline{Sh}_R / Sh_0) / (f/f_0)^{1/3} \quad (9)$$

NUMERICAL SIMULATION

The numerical simulations were conducted to understand the flow field in the stationary passage. The computation domains are modeled for the geometry of the experimental square duct (AR = 5.0) with rib turbulators and operating conditions are also in accordance with those of the experimental study. A commercial package program (FLUENT 12.1) was used to calculate flow fields and computation domain grids were created using GAMBIT solid modeling. The Reynolds number based on hydraulic diameter is 10,000. At the outlet of the channel, boundary condition was defined as pressure-outlet. Although different grids with 1,000,000 ~ 5,000,000 cells were tested to verify the grid independence of the solution, remarkable differences in the solutions were not observed. The grid model was met by $y^+ \leq 4$ for the first grid point near the wall. A smooth outlet section with a length of $2D_h$ was included in order to avoid an influence of reversed flow on the main area of interest. The fluid flow is calculated using an RNG (re-normalization group) $k - \epsilon$ turbulent model with non-equilibrium wall functions for the near-wall treatment.

RESULTS AND DISCUSSION

Effect of Guide Vanes

Figure 6 shows the conceptual secondary flow structure in the stationary duct. For flow without rotation, the velocity profile in the first passage was found to have a symmetric distribution. When the coolant flow passed through the turning region (Figure 6(b)-B), a pair of counter-rotating-vortex cells, known as Dean vortices, was generated due to the duct curvature. These vortices enhanced the heat transfer in the turning region and the entrance to the second passage. The effect of the Dean vortices was sustained along the second passage, but diminished in the downstream region (Figure 6(b)-D). Kim et al. [13] explained these results in detail, and their flow patterns are in good agreement with the results of this study.

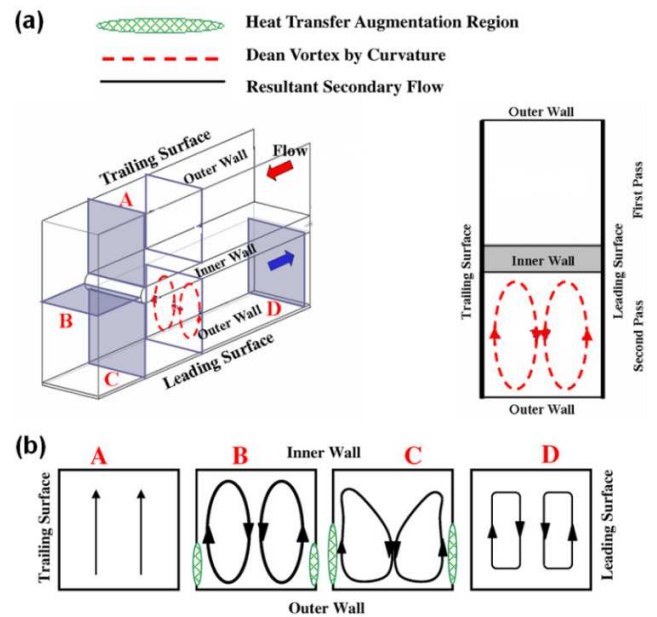


Figure 6. Expected secondary flow patterns in the two-pass duct: (a) conceptual secondary flow structures, (b) secondary flows for different location. [13]

Figure 7(a) shows the heat/mass transfer distribution on the duct surface and the tip surface in the case of no guide vanes. The results for the leading and trailing surfaces of a stationary duct are the same, so only the leading surface is discussed. The heat/mass transfer properties were reflected by the flow characteristics in the two-pass duct. The local heat/mass transfer coefficients of the duct surface in the first passage decreased towards the downstream, due to the fully developed turbulent flow from the duct inlet. The flow was separated by the divider wall while passing through the turning region, and generated a recirculation zone, located near the corners on both sides. In this region, the local heat/mass transfer was very low. However, the heat transfer was enhanced near the divider wall in the turning region, due to the Dean vortices. As noted above, the Dean vortices appeared in the turning region, and were coupled together in the recirculation flow. Thus, the coolant flow impinged on the duct surface, and the heat transfer was also enhanced near the divider wall in the turning region. The high-momentum core flow formed a pressure gradient at the outer wall, and a reversed pressure gradient at the inner wall of the inlet to the second passage, due to the centrifugal force generated by the flow passing through the turning region. The accelerated high-momentum flow was concentrated on the outer wall of the inlet to the second passage. Thus, the region near the outer wall of the second passage had locally high heat/mass transfer coefficients. However, the main flow was separated from the inner wall, so that a turn-induced separation bubble was also created near the divider wall. The separation bubble caused low heat transfer near the divider wall in the second passage.

Incoming flow from the duct inlet impinging on the first-pass side of the tip surface. Thus, the heat/mass transfer coefficient was very high on the first-pass side of the tip surface. A recirculation flow was generated along the tip surface after passing the impingement zone, and the heat/mass transfer coefficient decreased in this section. The heat/mass transfer coefficient on the tip surface at $y/D_h \approx 6$ was slightly increased. A counter-rotating-vortex appeared and enhanced the heat transfer in this region, because the main flow was turned towards the entrance to the second passage.

Figures 7(b)-(f) show the heat/mass transfer distributions with various guide vane configurations. Generally, the heat/mass transfer characteristics of the turning region and the

second passage were altered by the presence of the guide vanes in turning region. Figure 7(b) shows the results with an inner guide vane on the second-pass side (2PIV). When the guide vane was located in front of the entrance to the second passage, the heat transfer near the divider wall in the second passage was enhanced. The turning flow was separated by the guide vane. The flow inside the guide vane was accelerated, and entered the second passage. This was the main turning flow separation, and it enhanced the heat transfer in the guide vane region and near the divider wall in the second passage. However, the heat transfer near the outer wall in the second passage decreased, because of the separation of the turning flow. The main turning flow turned near the tip surface on account of the guide vane.

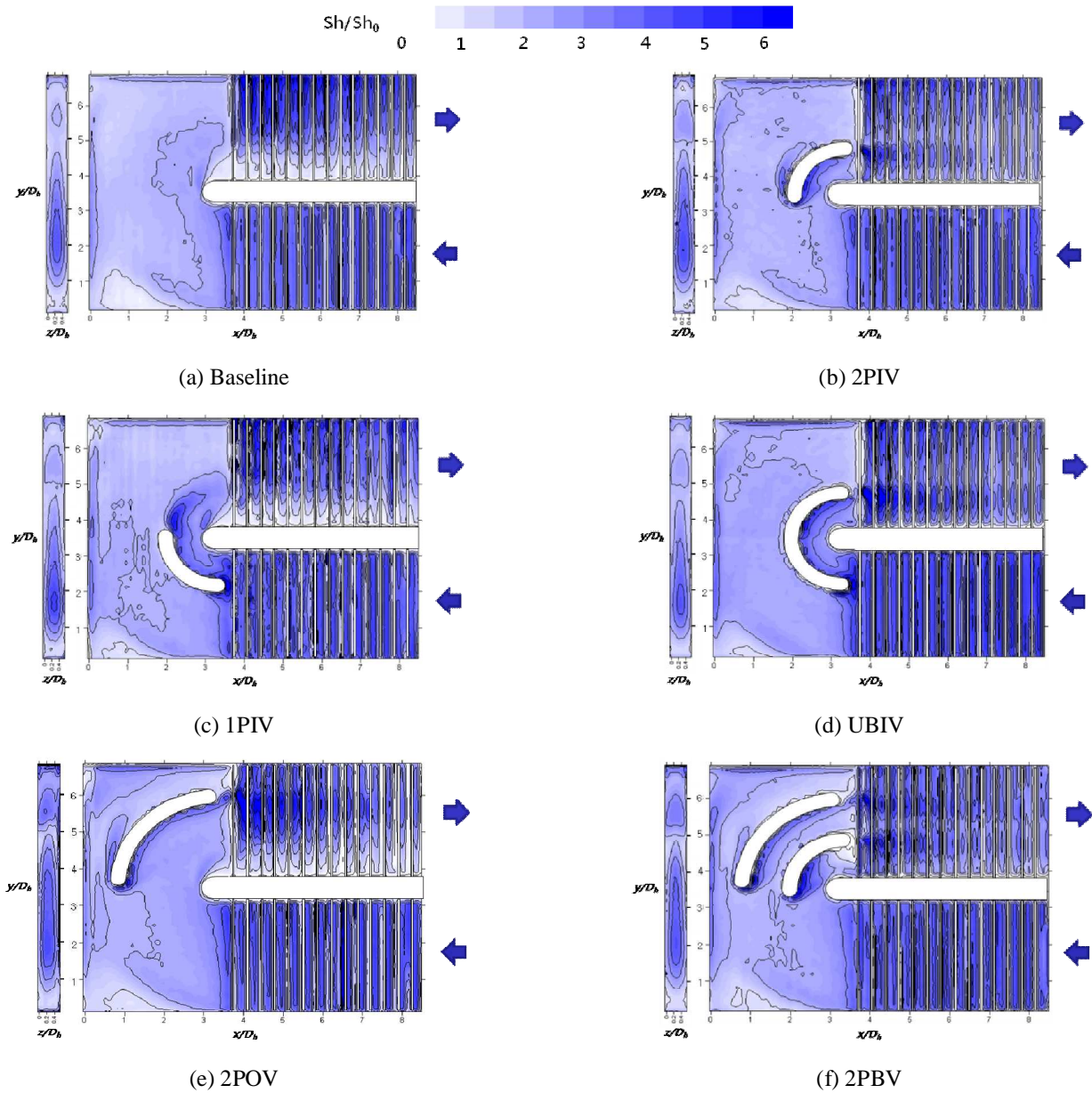


Figure 7. Heat/mass transfer distribution on the duct and tip surfaces for various guide vanes.

The effect of the Dean vortices on the tip surface and in the turning region was stronger and broader than in the baseline case. Thus, the stalled flow zone, located in the corner of the second-pass side of the turning region, was reduced, and the heat transfer increased in this region.

Figures 7(c) and (d) show the results with a guide vane on the first-pass side (1PIV) and in the U-bend (UBIV). In the 1PIV case, the overall heat transfer on the duct surface was not enhanced. The flow was separated in the outlet of the first passage. The separated flow slightly enhanced the region at the end of the guide vane. However, the part of the flow that passed inside the first guide vane mixed with main turning flow and broke up the Dean vortices in the turning region. Thus, the separated flow did not reduce the separation region near the divider wall in the second passage, and the heat transfer decreased near the outside wall in second passage. The Dean vortices turned near the tip surface. Thus, the heat transfer increased slightly in comparison to the baseline case. The UBIV case also exhibited no significant change in heat transfer. Heat transfer in the turning region and on the tip surface was similar to that of the base case. The separation region near the

divider in the second passage was reduced by the flow passing through the inside of the guide vane in the U-bend. There was increased uniformity of heat transfer in the second passage.

Figure 7(e) shows the results with an outer guide vane on the second-pass side (2POV). Again, the turning flow was separated by the guide vane. The stalled flow zone on the second-pass side disappeared because of the separated flow. The separated flow enhanced the heat transfer on the tip surface and in the turning region. High heat transfer occurred in the middle of the entrance to the second passage. The flow separation region near the divider wall in the second passage was broader than in the 2PIV case. The heat transfer near the outside wall of the second passage was lower than in the baseline case. The outer guide vane on the second-pass side enhanced the heat transfer on the tip surface and in the turning region.

Figure 7(f) shows the heat transfer distribution in the second passage with both guide vanes (2PBV). This case combined the advantages of 2PIV and 2POV. High heat transfer appeared on the tip surface and in the turning region. The separation region in the second passage was reduced. The heat

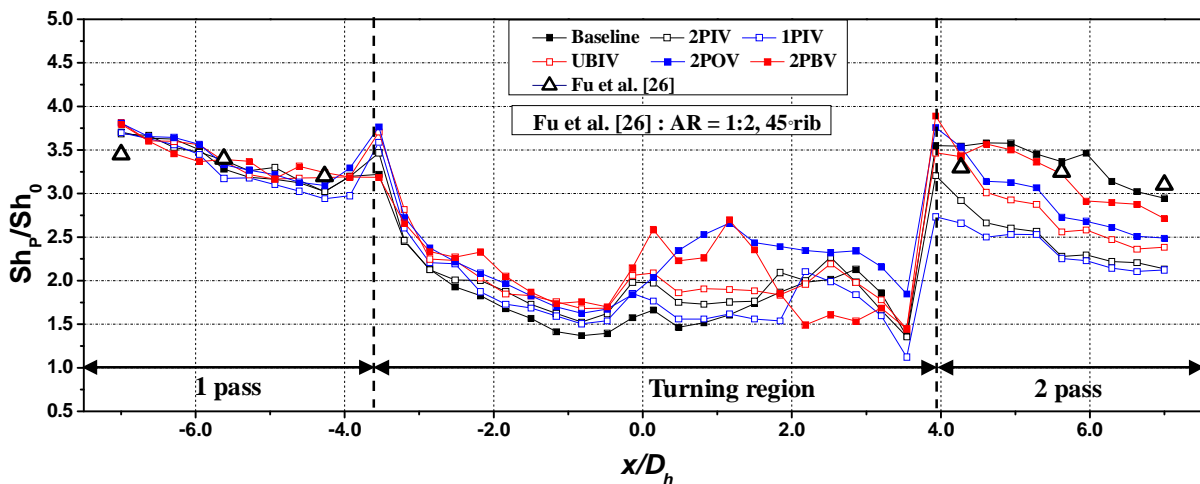


Figure 8. Pitch-wise averaged Sherwood number on the duct surface for various guide vanes.

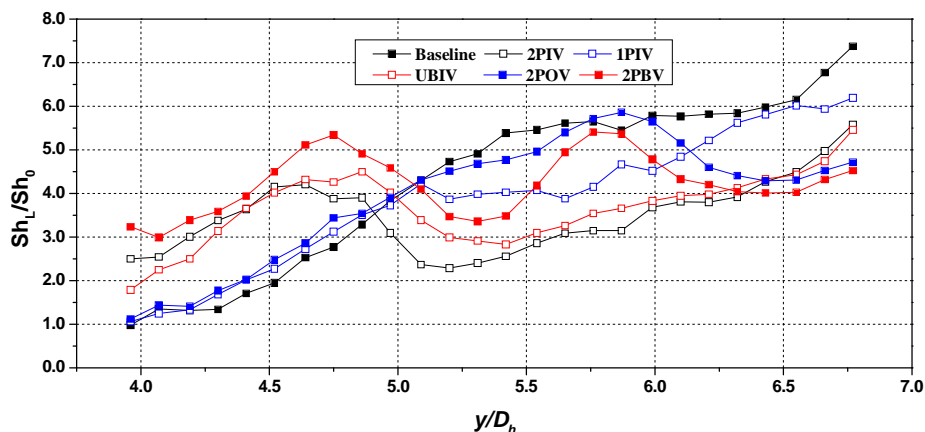


Figure 9. Local Sherwood number at the third pitch on the duct surface for various guide vanes. (at $x/D_h = 4.59$)

transfer in the second passage was more uniform than in the other cases. However, because the turning flow was divided by two guide vanes, the size of the Dean vortices was reduced. Thus, the peak heat transfer value was lower than those of 2PIV and 2POV.

Figure 8 shows the pitch-averaged Sherwood number ratio of the duct surface. The results were in good agreement with the experimental results of Fu et al. [26]. The average heat transfer coefficients in the turning region of the first-pass side were slightly higher with the guide vanes than in the baseline case. However, the heat transfer in the turning region of the second-pass side varied significantly in each case. In general, the guide vane cases had high heat transfer compared with the baseline, due to the flow impingement on the guide vane and the vortex generated by flow separation at the end of the guide vane. In particular, 2POV produced much higher average heat transfer coefficients in this region than the other cases. In the 2PBV case, the turning flow was smooth, and the Dean vortices lose the strength quickly. As a result, the heat transfer decreased beyond $x/D_h \approx 2$.

Generally, the average heat/mass transfer coefficient was decreased by the presence of a guide vane on the second-pass. The turning flow induced secondary vortices (such as the Dean vortices), but these vortices were not strongly developed in the turning region due to the guide vane. The guide vane separated the turning flow and broke up the secondary vortices. Thus, the heat transfer was lower in the various cases with guide vanes on the second-pass compared with the baseline case.

In the 2POV case, enough of the turning region was inside the outer guide vane region to enable the turning flow to develop and induce the secondary vortices. Part of the flow passed outside the outer guide vane, and thus high heat transfer occurred at the first pitch of the second passage and in the turning region.

In the 2PBV case, the average heat/mass transfer coefficient in the second passage was at the same level as the baseline case. The turning flow was smooth and accelerated, due to the narrowness of the turning passage. This accelerated turning flow enhanced the heat transfer at the first pitch of the

second passage. However, the heat/mass transfer coefficient in the second passage was lower in the 2PBV case than in the baseline case from the seventh pitch.

Figure 9 shows the local Sherwood number (Sh_L) at the third pitch of the second passage ($x/D_h = 4.59$). In the 2PIV, 2PBV and UBIV cases, the heat/mass transfer distribution in the second passage was uniform, due to the decreasing flow separation in the turning region. In each of these cases, the local Sherwood number ratio increased between $y/D_h \approx 4$ and $y/D_h \approx 5$, at the third pitch of the second passage ($x/D_h = 4.59$). The 2PIV and UBIV cases had fairly uniform local Sherwood number ratio at the third pitch of the second passage, but the ratio was the low, due to the diminishing secondary flow. In the 2PBV case, uniform heat transfer was achieved in the second passage, and the average heat/mass transfer coefficient remained at the same level throughout the passage. In the 1PIV case, the local Sherwood number ratio remained at the same level with the baseline case between $y/D_h \approx 4$ and $y/D_h \approx 5.2$. However, due to the weakened secondary flow, the ratio was lower than in the baseline case from $y/D_h \approx 5.2$ onward. In the 2POV case, the local Sherwood number ratio remained at the same level with the baseline case between $y/D_h \approx 4$ and $y/D_h \approx 6$, but the secondary flow was also broken by the guide vane. Thus, the ratio decreased from $y/D_h \approx 6$ onward.

Figure 10 shows the span-wise averaged Sherwood number ratio of the tip surface. As previously noted, the incoming flow from the duct inlet impinged on the first-pass side of the tip surface. Thus, the heat/mass transfer coefficient was very high on the first-pass side of the tip surface. Also, the heat/mass transfer coefficient on the tip surface increased around $y/D_h = 5.8$. A counter-rotating-vortex occurred, enhancing the heat transfer in this region, because the main turning flow turned towards the entrance to the second passage.

The overall heat transfer on the tip surface was enhanced by the presence of the guide vanes, because the flow reaching the tip surface was strengthened by the shorter circulation range of the Dean vortices. The turning flow was separated by the guide vanes, and part of the flow was steered to the outside of the guide vanes. This flow enhanced the heat transfer on the tip

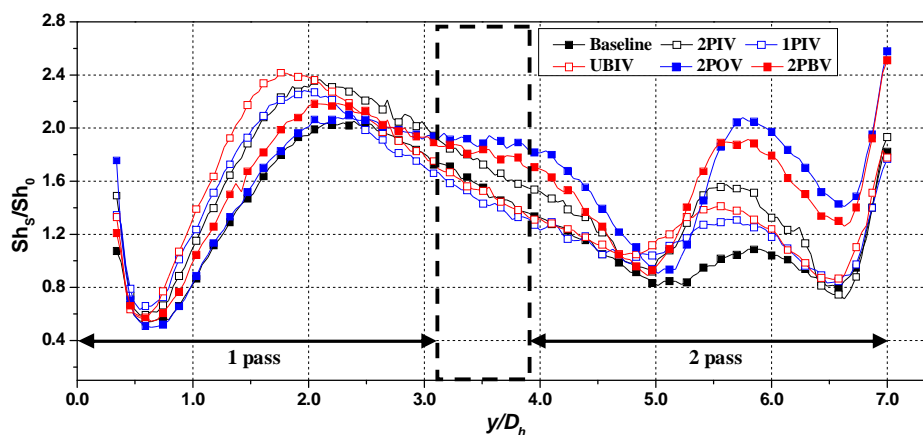


Figure 10. Span-wise averaged Sherwood number on the tip surface for various guide vanes.

Table 1 Summary of overall average Sh/Sh_0

	Baseline	2PIV	1PIV	UBIV	2POV	2PBV
1pass	3.33	3.37	3.30	3.42	3.43	3.37
Turning	1.76	1.90	1.80	1.98	2.18	2.06
2pass	3.07	2.44	2.21	2.61	2.90	2.93
Tip	1.27	1.50	1.40	1.46	1.60	1.57

surface.

The heat transfer on the tip surface was especially enhanced when the guide vane was installed on the second-pass side of the turning region. The separated flow produced by the guide vane and the counter-rotating-vortex arising from the turning flow enhanced greatly the heat transfer on the second-pass side of the tip surface. By changing the location of the guide vane from the inner to the outer side, the heat transfer was further enhanced and made uniform on the tip surface. The heat/mass transfer coefficient on this downstream region was the highest in the 2POV case.

Table 1 summarizes the total averaged Sherwood number ratios for each case. The table indicates that the total average Sherwood number ratio on the tip surface is enhanced by about 26% and 24% with 2POV and 2PBV, respectively.

Figure 11 shows the friction factor ratios, ff_0 , for various guide vanes. The friction factor ratio was lower with the guide vanes except the 2POV case. In detail, the reduction rates of ff_0 are about 12% and 14% from the base case for 2PIV and UBIV, respectively. UBIV is the lowest case of pressure loss. However, the friction factor ratio was increased about 5% for the 2POV case. And, the friction factor ratios of numerical calculation match well those of experiments.

It is evident that the presence of a guide vane improves substantially the flow distribution through the turning region, particularly in the downstream. The downstream flow separation is reduced at the end of turning region with the guide vanes. Indeed, it shows more uniform flow distribution in the entrance of the second pass. The guide vanes also modify the vortex structure in the turning region and the second-pass. The vortex structure and strength are changed significantly with the guide vanes. Therefore, the friction loss is reduced for some cases because the flow separation and vortex generation have been changed with the guide vanes.

The thermal performance factors, η (Eq. 10), obtained from a constant pumping power are presented in Figure 12. The thermal performance factor was increased with the guide vane except 1PIV. The thermal performance factor of 1PIV was decreased about 8%, and the thermal performance factor was increased about 3% and 4.5% with UBIV and 2POV, respectively. 2PBV has the highest thermal performance factor, which is about 8% enhancement.

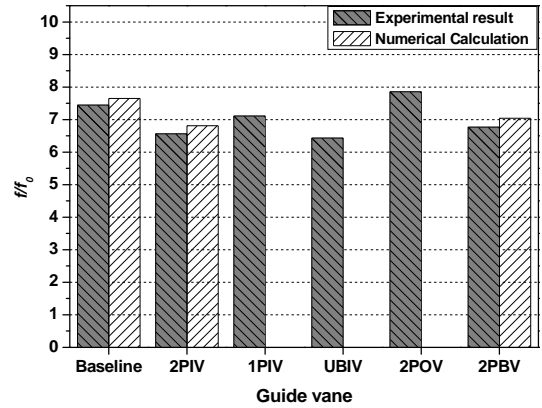


Figure 11. Friction factor ratios for various guide vanes.

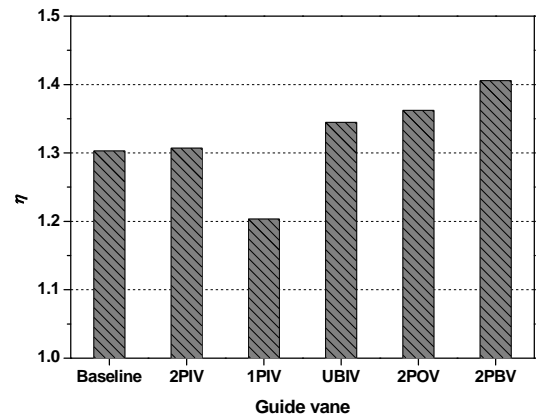


Figure 12. Thermal performance factors for various guide vanes.

Flow Patterns

The major factors that influence the heat transfer characteristics in a two-pass duct with guide vanes are the Dean vortices, disturbed flow by guide vanes, and turbulent flow on the duct surfaces. Those are related to the curvature of turn geometry, guide vanes and 90°-ribs, respectively. Those components result in complicated flow patterns, local heat transfer augmentation and overall heat transfer uniformity.

Figure 13 presents velocity contour plots on the duct at $z/D_h = 0.12$ for various guide vanes in the tip turn region. The velocity profiles in the first-pass are observed having uniform distributions. The separated flow at the tip of the divider wall was reduced by the guide vanes. Consequently, the results of numerical simulation were qualitatively in good agreement with the experimental results (Figure 7).

Figure 14 shows vorticity contours in the turning region for various guide vanes. When the coolant fluid flows pass the turning region at the baseline case (A-O line, Figure 14), a pair of counter-rotating-vortex cells, “Dean vortices” are produced due to the duct curvature, and the core flow moves from the middle of the duct to the outer wall. At the entrance of the second pass ($x/D_h = 3.5$, B-O line), the main flow is

separated from the inner wall so that a turn-induced separation bubble is additionally created near the divider wall (inner wall). When the flows pass the turning region with guide vanes (2PIV and 2PBV; A-O line, Figure 14), the turning flow was disturbed by the guide vanes. So, the Dean vortices are divided and the size of the Dean vortices was reduced. These changed vortex patterns affect significantly the friction loss and heat transfer in the turning region. At the entrance of the second pass with 2PIV and 2PBV ($x/D_h = 3.5$, B-O line), the separation bubble was reduced and the divided Dean vortices were scattered. As a result, the heat transfer rate at the entrance of the second pass was uniformed.

CONCLUSION

Mass transfer experiments were conducted to understand the effects of guide vanes in a two-pass duct. Five different guide vane configurations were used to investigate the changes in heat/mass transfer characteristics and pressure drop caused by the guide vane location. The local Sherwood number ratio distributions (Sh/Sh_0) explicitly reveal the heat/mass transfer phenomena, especially the augmentation on the surfaces where the vortices impinge. Under the present experimental and geometric conditions, it can be concluded that guide vanes in the turning region enhance the heat/mass transfer, by controlling the Dean vortices and flow separation.

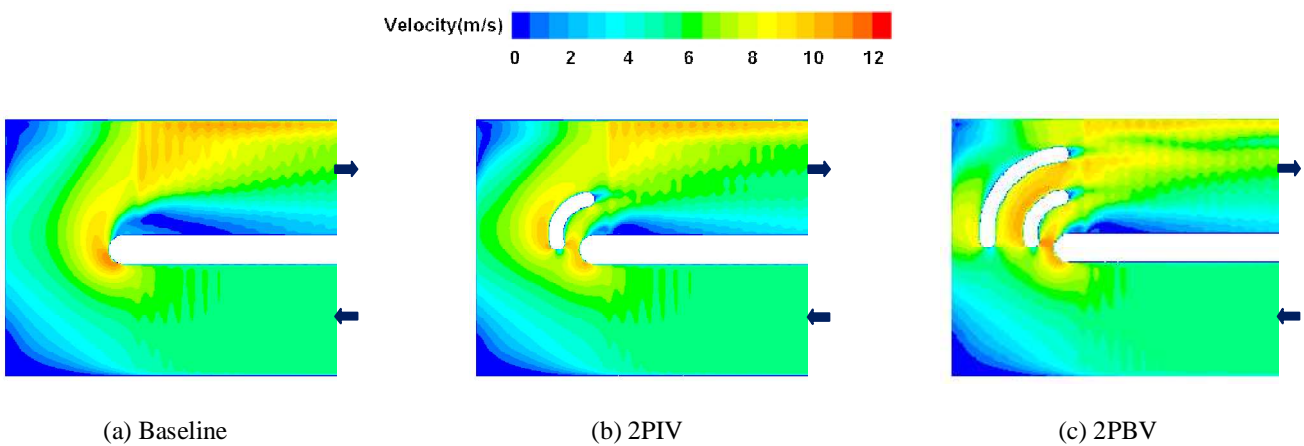


Figure 13. Velocity contours on the duct for various guide vanes. (at $z/D_h = 0.12$)

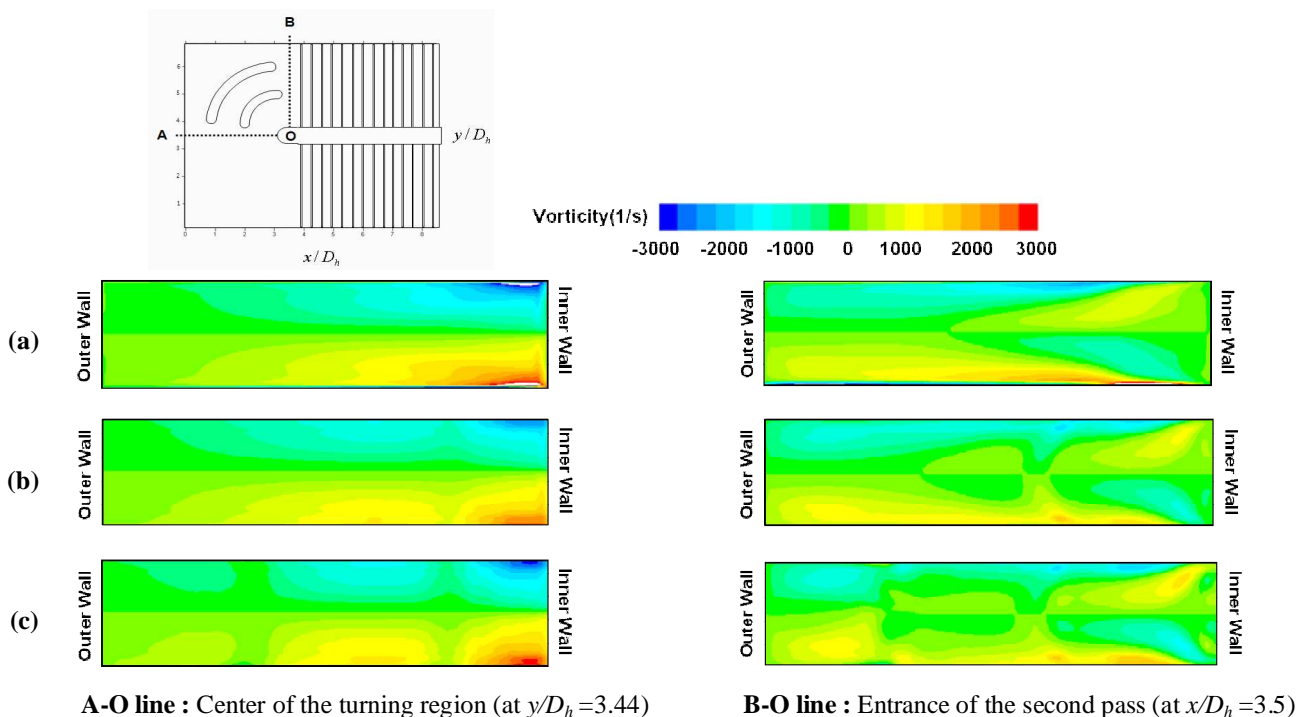


Figure 14. Vorticity contours in the duct; (a) Baseline, (b) 2PIV, (c) 2PBV.

1. In the first passage, a guide vane in the turning region produced no change. In the second passage, the heat transfer was decreased by the presence of the guide vane. However, by using 2PBV, it is possible to reduce the amount by which the average heat/mass transfer coefficient is decreased in the second passage. And, 2PBV is the best case for thermal performance. The increment rate of thermal performance factor is about 8% compared to the baseline case.
2. When a guide vane is placed on the second-pass side, the heat/mass transfer distribution in the second passage is made uniform, due to the decreasing flow separation in the turning region.
3. On the tip surface, the overall heat/mass transfer is increased by a guide vane, due to the enhanced impingement effect of the Dean vortices. In the case of 2POV and 2PBV, the total average Sherwood number ratio on the tip surface was enhanced by 26% and 24% over the case in which no guide vane is used, respectively.

NOMENCLATURE

C_p	Specific heat (J/kgK)
D_h	Hydraulic diameter (mm)
D_{naph}	Mass Diffusion coefficient of naphthalene vapor in air (m^2/s)
f	Friction factor
f_0	Friction factor of a fully developed turbulent flow in a stationary smooth pipe
H	Duct height (mm)
k	Thermal conductivity (W/mK)
L	Channel length (mm)
Nu	Nusselt number (hD_h/k_c)
P_{naph}	Naphthalene vapor pressure (N/m ²)
Pr	Prandtl number ($\mu C_p/k$)
Re	Reynolds number ($U D_h/\nu$)
R_{naph}	Naphthalene gas constant (J/molK)
Sc	Schmidt number (ν_{air}/D_{naph})
Sh	Sherwood number ($h_m D_h/D_{naph}$)
Sh_0	Sherwood number, Eq. (6)
Sh_L	Local Sherwood number
Sh_p	Pitch-wise averaged Sherwood number
Sh_s	Span-wise averaged Sherwood number
T_w	Wall temperature (K)
U	Test section inlet velocity (m/s)
W	Duct width (mm)
μ	Dynamic viscosity (kg/ms)
ν	Kinematic viscosity (m^2/s)
e	Rib height (mm)
p	Distance of the rib pitch (mm)
x	Coordinate and distance in the streamwise direction (mm)

y	Coordinate and distance in the lateral direction (mm)
z	Coordinate and distance in the vertical direction (mm)
h_m	Mass transfer coefficient (m/s)
\dot{m}	Local naphthalene mass transfer rate per unit area (kg/m^2s)
η	Thermal performance, Eq. (9)
ρ_s	Density of solid naphthalene (kg/m^3)
$\rho_{v,w}$	Vapor density of naphthalene on the surface (kg/m^3)
$\rho_{v,b}$	Vapor density of bulk air (kg/m^3)
Δz	Sublimation depth of naphthalene surface (mil)
Δt	Runtime (s)
\dot{Q}_{air}	Volume flow rate of air (m^3/s)
$z_{sub} x$	Average sublimation depth of naphthalene surface (mil)

ACKNOWLEDGMENTS

This work was supported by the Power Generation & Electricity Delivery of the Korea Institute of Energy Technology Evaluation and Planning (KETEP) grant funded by the Korea government Ministry of Knowledge Economy. (No.2009T100200077)

REFERENCES

- [1] Lakshminarayana, B., 1996, *Fluid Dynamics and Heat Transfer of Turbomachinery*, John Wiley and Sons, New York.
- [2] Bunker, R. S., 2001, "A Review of Turbine Blade Tip Heat Transfer," *Annals of the New York Academy of Sciences*, Vol. 934, pp. 64-79.
- [3] Sunden, B., Xie, G., 2010, "Gas Turbine Blade Tip Heat Transfer and Cooling: A Literature Survey," *Heat Transfer Engineering*, Vol. 31, No. 7, pp. 527-554.
- [4] Park, J. S., Han, J. C, Huang, Y., and Ou, S, 1992, "Heat Transfer Performance Comparisons of Five Different Rectangular channels with parallel Angled Ribs," *Int. J. Heat Transfer*, Vol. 35, No. 11, pp. 2891-2903.
- [5] Han, J. C., Chandra, P. R., and Lau, S. C., 1988, "Local Heat/Mass Transfer Distributions Around Sharp 180 Deg Turns in Two-Pass Smooth and Rib-Roughened Channels," *Int. J. Heat Transfer*, Vol. 110, pp. 91-98.
- [6] Cardone, G., Astarita, T., and Carlomagno, G. M, 1995, "Surface Flow Visualization Around a 180 Deg Turn Channel for Different Aspect Ratios," *In Flow Visualization VIII*, Crowder J. ed., Begell House, pp. 977-982.
- [7] Astarita, T, Cardone, G., and Carlomagno, G. M, 1998, "Average Heat Transfer Measurements Near a Sharp 180 Degree Turn Channel for Different Aspect ratios," *Proceedings of IMECHE Conference Transactions*, Mechanical Engineering Publications, pp. 137-146.
- [8] Mochizuki, S., Murata, A., Shibata, R., and Yang, J. W., 1999, "Detailed Measurements of Local Heat Transfer Coefficients in Turbulent Flow Through Smooth and Rib-Roughened Passages with a 180 Sharp Bend", *Int. J. Heat and*

Mass Transfer, Vol. 42, pp. 1925-1934.

[9] Kim, K. M., Lee, D. H., and Cho, H. H., 2007, "Detailed Measurement of Heat-Mass Transfer and Pressure Drop in a Rotating Two-Pass Duct With Transverse Ribs," *Int. J. Heat and Mass Transfer*, Vol. 43, pp. 801-815.

[10] Kim, K. M., Lee, D. H., Rhee, D. H., and Cho H. H., 2006, "Local Heat/Mass Transfer Phenomena in Rotating Passage, Part 1: Smooth Passage," *AIAA Journal of Thermophysics and Heat Transfer*, Vol. 20, No. 2, pp. 188-198.

[11] Kim, K. M., Lee, D. H., Rhee, D. H., and Cho, H. H., 2006, "Local Heat/Mass Transfer Phenomena in Rotating Passage, Part 2: Angled Ribbed Passage," *AIAA Journal of Thermophysics and Heat Transfer*, Vol. 20, No. 2, pp. 199-210.

[12] Kim, K. M., Lee, D. H., and Cho, H. H., 2007, "Rotational Effects on Pressure Drop in Smooth and Ribbed Two-Pass Ducts," *AIAA Journal of Thermophysics and Heat Transfer*, Vol. 21, No. 3, pp. 644-647.

[13] Kim, K. M., Kim, Y. Y., Lee, D. H., Rhee, D. H., and Cho, H. H., 2007, "Influence of duct aspect ratio on heat/mass transfer in coolant passages with rotation," *Int. J. Heat and Fluid Flow*, Vol. 28, pp. 357-373.

[14] Cho, H. H. Lee, S. Y., and Rhee, D. H., 2004, "Effects of Cross Ribs on Heat/Mass Transfer in a Two-Pass Rotating Duct," *Int. J. Heat and Mass Transfer*, Vol. 40, pp. 743-755.

[15] Zehnder, F., Schuler, M., Weigand, B., Wolfersdorf, J. V., and Neumann, S. O., 2009, "The Effect of Turning Vanes on Pressure Loss and Heat Transfer of a Ribbed Rectangular Two-Pass Internal Cooling Channel," *ASME paper No. GT2009-59482*.

[16] Bunker, R. S., 2007, "The Augmentation of Internal Blade Tip-Cap Cooling by Arrays of Shaped Pins," *ASME paper No. GT2007-27009*.

[17] Tareq, S., Sunden, B., 2010, "An Experimental Study of heat Transfer and Pressure Drop on the Bend Surface of a U-duct," *ASME paper No. GT2010-22139*.

[18] Xie, G. N., Sunden, B., Wang, Q., 2010, "Predictions of Enhanced heat Transfer of an Internal Blade Tip-Wall with Hemispherical Dimples or Protrusions," *ASME paper No. GT2010-22265*.

[19] Jeon, Y. H., Park, S. H., Kim, K. M., Lee, D. H., and Cho, H. H., 2007, "Effects of Bleed Flow on Heat/Mass Transfer in a Rotating Rib-Roughened Channel," *ASME J. Turbomachinery*, Vol. 129, pp. 636-642.

[20] Ambrose, D., Lawrenson, I. J. and Sparke, C. H. S., 1975, "The Vapor Pressure of Naphthalene," *J. Chem. Thermodynamic*, Vol. 7, pp. 1173-1176.

[21] Goldstein, R. J., and Cho, H. H., 1995, "A Review of Mass Transfer Measurements Using Naphthalene Sublimation," *Experimental Thermal and Fluid Science*, Vol. 10, pp. 416-434.

[22] McAdams, W. H., 1942, *Heat Transmission*, 2nd ed., McGraw-Hill, New York.

[23] Moffat, R. J., 1988, "Describing the Uncertainties in Experimental Results," *Experimental Thermal and Fluid Science*, Vol. 1, No. 1, pp. 3-17.

[24] Petukhov, B. S., 1970, *Advances in Heat Transfer*, Vol. 6, pp. 503-504, Academic Press, New York.

[25] Griggull, U., Hahne, E., editors. 1969, *Progress in heat and mass transfer*, Vol. 1, pp. 331, Oxford: Pergamon Press.

[26] Fu, W. L., Wright, L. M., Han, J. C., 2005, "Heat Transfer in Two-Pass Rotating Rectangular Channels (AR = 1:2 and AR = 1:4) with 45 Deg Angled Rib Turbulators", *ASME J. Turbomachinery*, Vol. 127, pp. 164-174.